Multi-hazard Earthquake-Tsunami Structural Fragility Assessment Framework

Mohammad S. Alam
Graduate Student Researcher, Oregon State University, Corvallis, OR, USA, 97331

Andre R. Barbosa
Associate Professor, Oregon State University, Corvallis, OR, USA, 97331

Michael H. Scott
Professor, Oregon State Univ., Corvallis, OR, USA, 97331

Daniel T. Cox
Professor, Oregon State University, Corvallis, OR, USA, 97331

John W. van de Lindt
Professor, Colorado State University, Fort Collins, CO, USA, 80523

ABSTRACT:

A probabilistic multi-hazard earthquake-tsunami fragility assessment framework is presented, which accounts for the effect of accumulated damage on the structure due to earthquake loading on its subsequent tsunami response. The fragility assessment framework involves simulating structural response using advanced three dimensional (3D) nonlinear finite-element structural model subjected to sequential earthquake-tsunami loading at multiple seismic and tsunami intensity levels, using back to back nonlinear response history analyses (NRHA) and nonlinear static pushover (NSP) analyses. A modern earthquake-tsunami code designed four story reinforced concrete (RC) special moment resisting frame (SMRF) building is used as an application example to illustrate the proposed framework. Results indicate that the effect of accumulated damage due to earthquake loading is more pronounced in reducing the stiffness of the structure compared to the reduction in structural capacity. Moreover, the tsunami structural capacity required to achieve a given probability of damage exceedance decreases with increasing seismic intensity, especially at lower damage states.

1. INTRODUCTION

Catastrophic events such as the Japan Tohoku Earthquake and Tsunami (2011) raised the global awareness for the need to understand the response of communities and the built environment to multi-hazard extreme events. Extreme events that produced significant damage and loss of life over the last two decades include the following earthquake and tsunamis: Indian Ocean (2004), Samoa (2009), Chile (2010), and Japan (2011). With respect to these extreme events, the majority of the devastation was sustained along the coastline, highlighting the importance of the damage produced by earthquake ground shaking and the following tsunami inundation.

Following the recent catastrophic tsunami events, many empirical fragility functions (Peiris, 2006; Charvet et al., 2014; Suppasri et al., 2015) have been developed to assess the performance of differ-

ent building classes based on post-tsunami survey of damaged structures. These functions are presented solely as tsunami fragility functions in the literature, with the assumptions that earthquake induced damage are minimal compared to tsunami induced damage. Though the validity of this assumption is questionable, the practice continues since it is not easy to distinguish between earthquake and tsunami damage sustained by a structure during post-tsunami survey. Significant advances have also been made recently in analytical tsunami fragility function development (Attary et al., 2017; Petrone et al., 2017; Alam et al., 2018), specifically for far-field tsunamis, where the response and damage of pristine structure subjected to tsunami loading is simulated through numerical simulations.

At present, there are only a few studies (Park et al., 2012; Latcharote, 2015; Carey et al., 2018) in the literature that evaluated structural performance under sequential earthquake shaking and tsunami inundation hazard. Park et al. (2012) developed collapse fragility functions for a two-story timber building subjected to sequential earthquake-tsunami loading in a two phase simulation performed at two seismic intensity levels. In the first phase, nonlinear response history analyses (NRHA) were performed using an equivalent single degree of freedom (SDOF) model of the timber building. In the second phase, tsunami response of the damaged SDOF model was evaluated through nonlinear static pushover (NSP) analyses for different inundation levels. The study observed that tsunami inundation depths required to collapse the assessed light-frame timber building decreased with increase in the seismic intensity of the preceding earthquakes. Latcharote (2015) performed sequential NRHA analyses to simulate the earthquake-tsunami response of a six-story reinforced concrete (RC) wall-frame structure and monitored damage of beam, column, and structural wall. The study found that damage accumulates in structural members during sequential earthquake-tsunami loading. Recently, Carey et al. (2018) developed a bridge modeling approach, which includes soil-foundation-structure interaction effects, to quantify sequential earthquake-tsunami induced damage. The study presented multi-hazard interaction diagram that relate earthquake and tsunami intensity measures (IMs) to bridge damage, which reveals that the effect of damage due to of earthquake loading on bridge systems decreases the resistance to subsequent tsunami loading.

Based on the literature review, it is evident that, at present, there is a lack of studies that systematically evaluate the effect of accumulated damage due to earthquake ground shaking on the increased vulnerability of structures under subsequent tsunami inundation in a probabilistic manner. To address this gap, this study presents a probabilistic framework to develop physics based multi-hazard earthquake-tsunami fragility functions, which can be used as a tool to assess structural risk and associated losses for structures vulnerable to near-field tsunamis. A four story reinforced concrete (RC) special moment resisting frame building (SMRF) designed per ASCE/SEI 7-16 (ASCE, 2016) and ACI 318-14 (ACI, 2014) is used as an application example to illustrate the proposed multi-hazard fragility assessment framework.

2. MULTI-HAZARD FRAGILITY ASSESSMENT FRAMEWORK

The multi-hazard fragility assessment involves assessing the response, represented by an engineering demand parameter (EDP), of the finite element model (FEM) of the structure to sequential earthquake-tsunami loading at several seismic and tsunami intensity levels, characterized by hazard intensity measures (IM). In this study, peak inter-story drift ratio (PIDR) is used as the EDP and spectral acceleration at the fundamental period of vibration $S_a(T_1)$ and specific momentum flux (hu^2), which includes information on tsunami inundation depth h and flow velocity u, are used as seismic and tsunami IM, respectively. An advanced three-dimensional (3D) nonlinear FEM of the structure is developed first in OpenSees to perform sequential earthquake-tsunami analyses. Since the uncertainties associated with both the hazards (ground motion (GM) record-to-record (RTR) variability and tsunami inundation depth-to-depth (HTH) variability) for a given intensity is of several fold mag-

nitude higher than that associated with model parameter uncertainties, RTR and HTH variability are explicitly considered in this framework by treating those hazard intensities as random variables, whereas all the model parameters and geometry are considered deterministic and set to their expected values.

2.1. Analysis framework

The sequential earthquake-tsunami analyses are performed in three stages:

(1) In the first stage, NRHA of the advanced 3D FEM under earthquake GM is performed. To perform NRHA, the TRBDF2 integrator object with a maximum analysis time step of 0.002 second is used in OpenSees. The Krylov-Newton alogrithm is used to solve the nonlinear system of equilibrium equations at each time step. The multiple-stripe analysis (MSA) approach is adopted to perform NRHA. In this study, six seismic IM levels are considered.

(2) In the second stage, the FEM is prepared for tsunami loading with its final state from the GM as the initial condition. To eliminate any structural vibration in the FEM, a transient analysis is performed for 10 seconds with fictitiously high equivalent viscous damping ratio of 30%.

(3) In the third stage, multiple NSP analysis are performed with tsunami hydrodynamic loading applied as uniformly distributed load on the columns of the structure in onshore direction irrespective of the leaning position of the damaged structure. In this study, six tsunami h levels up to third story roof level are considered, with minimum inundation being considered at mid-height of ground story. Though, other tsunami forces such as hydrostatic, buoyancy forces, and debris impact and damming forces can induce great damage in structures, those forces are not considered herein. The overall tsunami hydrodynamic force F_{dx} applied to the structure is given as (ASCE, 2016)

$$F_{dx} = \frac{1}{2} \rho_s C_d C_{cx} B(hu^2), \qquad (1)$$

where ρ_s = fluid density, C_d = drag coefficient for the building, B = overall building width perpendicular to the flow direction, h = tsunami inundation depth above the grade level, u = tsunami flow velocity at building site, and C_{cx} = closure coefficient, which is equal to 1.0 if no openings in the structure, perpendicular to the flow direction, are present. Following ASCE (2016) recommendation, $C_{cx} = 0.7$ is used in this study.

Throughout the analysis stages, PIDR and base shear response of the structure are monitored. Base shear response is converted to equivalent hu^2, which is used as the tsunami IM.

2.2. Fragility Assessment Framework

The proposed fragility assessment framework is an extension of the framework developed in Alam et al. (2018) for far-field tsunamis. The framework consists of performing the following steps:

(1) In step 1, multiple realizations of tsunami demand in terms of hu^2 are generated. To this end, at first, a suite of inundation depth h_i is randomly generated such that $h_i \in h \sim Unif[0, h_{max}]$, where h_{max} is the maximum plausible inundation depth at the building site. Then, for each h_i, a suite of velocity values $u_{i,j}$ is randomly generated such that $u_{i,j} \in u \sim Unif[0, U_{i,max}]$. The maximum velocity $u_{i,max}$ is constrained to ($U_{i,max} = F_r\sqrt{g.h_i}$) Froude number F_r, which is equal to 2.0 in this study. Finally, for each $(h_i, u_{i,j})$ pair, the tsunami demand intensity $im_{i,j}$ is computed as $h_i u_{i,j}^2$.

(2) In step 2, for a damage state ds_k, and for the given inundation depth h_i, the value of the peak structural capacity IM_{cap,i,ds_k} is interpolated from the multiple tsunami capacity curves corresponding to different h, which are obtained during the stage 3 of the analysis framework.

(3) In step 3, the demand computed in step 1 is compared against the structural capacity computed in step 2, to compute the failure indicator $Y_{i,j,ds_k} = \begin{cases} 1 & \text{if } im_{i,j} > IM_{cap,i,ds_k} \\ 0 & \text{Otherwise} \end{cases}$

3

Steps 1–3 are repeated until all h_i and $u_{i,j}$ combinations are exhausted for each sequential NRHA-NSP analysis.

(4) Finally, parameterized fragility functions are developed with Y_{i,j,ds_k} data using the logistic generalized linear model (GLM). The CDF of event $\{IM_{EQ_{cap}} > im_{EQ} \cap IM_{TSU_{cap}} \leq im_{TSU}\}$ conditional on a damage state ds_k and a set of basic random variables X can be computed as:

$$P[IM_{EQ_{cap}} > im_{EQ} \cap IM_{TSU_{cap}} \leq im_{TSU}|ds_k, \mathrm{X}]$$
$$= \frac{\exp(g[\mathrm{X}])}{1 + \exp(g[\mathrm{X}])} \quad (2)$$

where $IM_{EQ_{cap}}$ and $IM_{TSU_{cap}}$ represent structural capacity in terms of IM for earthquake and tsunami loading, respectively. Eq. (2) provides the joint probability of event where a given ds_k is not exceeded due to earthquake but exceeded due to subsequent tsunami effect. In this study, RTR of ground motions and HTH variability of tsunami inundation constitute the X vector.

3. APPLICATION EXAMPLE

3.1. Description of Application Example

A newly designed four-story RC office building, designed following ACI 318-14 (ACI, 2014) and considering seismic and tsunami loading as per ASCE/SEI 7-16 (ASCE, 2016), is utilized as an application example. Fig. 1 shows the overview of the the site and elevation view of an exterior frame in the E-W direction. The building is located close to the shoreline of the Pacific coast at Seaside, Oregon, USA. The building site is located in a high seismic zone as well as within the tsunami inundation zone in the event of a 2500 year maximum considered tsunami (MCT). The design spectral acceleration ordinates S_{DS} and S_{D1} are 0.87g and 0.77g at the site, respectively, as per the Conterminous U.S.2014 (v4.1.1) edition of the seismic hazard map. ASCE 7-16 compatible tsunami design IMs, h of 10.8 m, u of 7.2 m/s, and hu^2 of 159.4 m^3/s^2 corresponding to MCT are obtained from site-specific tsunami hazard analysis performed in Park et al. (2017). The typical bays are 9.15 m long

in North-South (N-S) direction and 6.1 m long in East-West (E-W) direction. The lateral load resisting system consists of SMRFs in both the N-S and E-W directions. Mat or spread footings are envisioned for the foundation system of the building, which is founded on a site class D soil (NEHRP). All columns are 76 cm x 76 cm. Level-2 beams are 60 cm x 86 cm, where as beams used in upper stories are 60 cm x 76 cm.

3.2. Numerical model

An advanced 3D FEM scheme for the application example building is developed in OpenSees. For columns and beams, material nonlinearity and geometric nonlinearity such as $P-\Delta$ effects are considered. Columns are modeled using an enhanced version of the distributed plasticity force-based fiber-section element by (Scott and Fenves, 2006), which allows for the nonlinear fiber sections assigned on the element interior contrary to the elastic interior described in original publication. Thus, moment-axial load interactions are explicitly considered in all columns. The plastic hinge length L_p was defined using the empirically validated relationship provided in Paulay and Priestley (1992). The uni-axial stress-strain response of concrete fibers are simulated using Scott et al. (1982) (*Concrete02*) and for reinforcing steel a bilinear stress-strain relationship (*Steel02*) with kinematic hardening ratio of 0.01 is used. The confinement effects are accounted for in the definition of the concrete stress-strain response by the Karthik and Mander (2010) confining model. To capture column shear failures, nonlinear zero-length shear springs are modeled at both ends of columns, near beam-column joints. For details on the shear spring models, see Alam et al. (2018).

Beams are modeled using force-based finite-length plastic hinge (FLPH) beam-column element (Scott and Fenves, 2006) together with a phenomenological hinge model with deterioration rules developed by Haselton et al. (2016). This empirical model is used to define the moment-rotation relationship of the plastic hinge region. The model's monotonic and hysteretic degradation rules allow to capture both post-peak in-cycle degradation, combined with cyclic deterioration. A $L_p = L/6$ (Scott and Ryan, 2013) is utilized for beams, which does
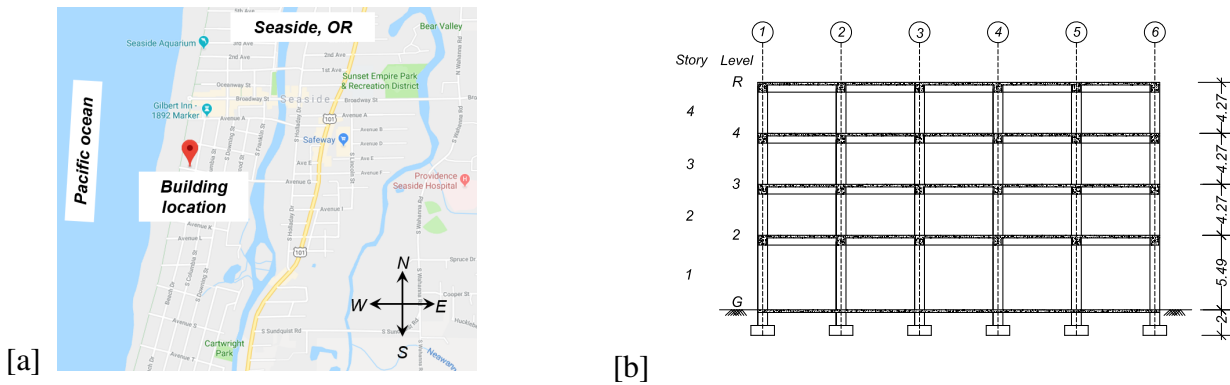
Figure 1: Application example: (a) overview of the building location, (b) elevation of an exterior frame in the E-W direction. All dimensions are in meters.

not correspond to physical plastic hinge length, but allows for perfect transformation of moment-rotation relationship to moment-curvature. The effective width of the flanged beam section is determined in accordance with ACI 318-14 (ACI, 2014). Beam-column joints are modeled using partially rigid-end offsets, following ATC-72-1 (PEER/ATC, 2010) recommendations.

Floor masses are lumped at beam-column joints. Gravity loads are assigned as uniformly distributed loading in beams. Rayleigh damping proportional to mass and current stiffness is assigned to the FEM considering 2% equivalent damping at the fundamental period T_1 and at the period corresponding to achieving 90% seismic mass participation. Eigen analyses of the 3D FEM was performed, which revealed that 90% seismic mass partition was achieved with first five vibration modes.The first three period of vibration are: $T_{N-S} = 0.86$ s, $T_{E-W} = 0.76$ s, and $T_{torsion} = 0.68$ s.

3.3. Ground motion selection

Chandramohan et al. (2016) and Barbosa et al. (2017) showed increased collapse risk of ductile RC frame structures located at sites prone to long duration GMs. As the application example building site's seismic hazard is dominated by interface earthquakes from the Cascadia Subduction Zone (CSZ), GMs are selected such that they satisfy response spectrum target as well as duration distribution target conditional on the response spectrum. Thus, a two step procedure is utilized for GM selection. In the first step, a large number of conditional

spectra (CS) compatible GMs are selected for six IM levels, corresponding to the $S_a(T_1, \xi = 5\%)$ exceedance probabilities of 10% in 50 years, 5% in 50 years, 2% in 50 years, 1% in 50 years, 0.67% in 50 years, and 0.5% in 50 years, using the GM selection algorithm by Baker and Lee (2018). Seismic hazard curves and deaggregation results of $S_a(T_1)$ are obtained from USGS unified hazard tools using the Conterminous U.S.2014 (v4.1.1) edition of the seismic hazard map for NEHRP site class D. $T_1 = 0.8$ second, which corresponds to the geometric mean of the first mode period of vibration of the two translational modes, is used for GM selection.

In the second step, from the large pool of selected CS compatible GMs, eleven ground motions are selected at each IM level such that they also satisfy the duration conditional distribution function target as well. In this study, Ds_{5-75} is used as an IM to represent GM duration, which represents the interval over which 5-75% of the $\int_0^{t_{end}} a^2(t)dt$ is accumulated, where $a(t)$ is the acceleration time history of GM. Source-specific Ds_{5-75} target distributions are computed following the formulations presented in Chandramohan et al. (2016). The Kolmogorov-Smirnov (K-S) goodness of fit test is utilized to check the adequacy of empirical duration CDF of selected GMs to that of Ds_{5-75} target distribution.

Fig. 2(a) and Fig. 2(b) show the CS compatible selected ground motions response spectrum and the duration distribution of selected GMs with the conditional Ds_{5-75} distribution target, respectively. Short duration GMs at lower end of the Ds_{5-75} scale in Fig. 2(b) are obtained from PEER

NGA-WEST2 database, whereas intermediate and long duration GMs are obtained from PEER NGA-WEST2 database, Belejo et al. (2017), and Long (2013).

3.4. Results

Using the multi-hazard earthquake-tsunami analysis framework presented above, a total of 396 sequential NRHA-NSP analyses are performed (6 seismic intensity level x 11 GMs x 6 tsunami inundation depth h). In the following sections results are presented.

3.4.1. Effect of seismic intensity on structural stiffness and capacity

Fig. 3(a) and Fig. 3(b) show the effect of GM induced accumulated damage on the stiffness and capacity of the building for the subsequent tsunami response, at seismic IM of 10% in 50 years $S_a(T_1)$ exceedance and 2% in 50 years $S_a(T_1)$ exceedance probability, respectively. In these figures, six distinct capacity curves (red dashed lines) corresponds to six inundation levels considered, with the highest hu^2 corresponding to lowest h at mid height of the ground story. At lower seismic IM (10% in 50 years exceedance level), minimal yet visible accumulated damage effect due to earthquake can be observed, which results in reduced initial stiffness and reduction in capacity of the structure compared to the undamaged structure's tsunami-only response. The accumulated damage effect is more pronounced at higher seismic intensity level (2% in 50 years exceedance level), which results in largely degraded initial stiffness along with reduction in structural capacity to a lesser extent.

3.4.2. Joint earthquake-tsunami fragility surface

Fig. 4 shows the joint earthquake-tsunami fragility contours for several probability levels for damage state corresponding to $PIDR > 2\%$. It can be observed that the specific hu^2 required to achieve a given probability of damage is a function of the seismic IM. Joint earthquake-tsunami fragility contours for 4%, and 6% PIDR exceedance levels are also developed, which reveal that with increasing seismic intensity, the hu^2 required to achieve similar probability of damage decreases, especially at lower damage state (2% PIDR exceedance).
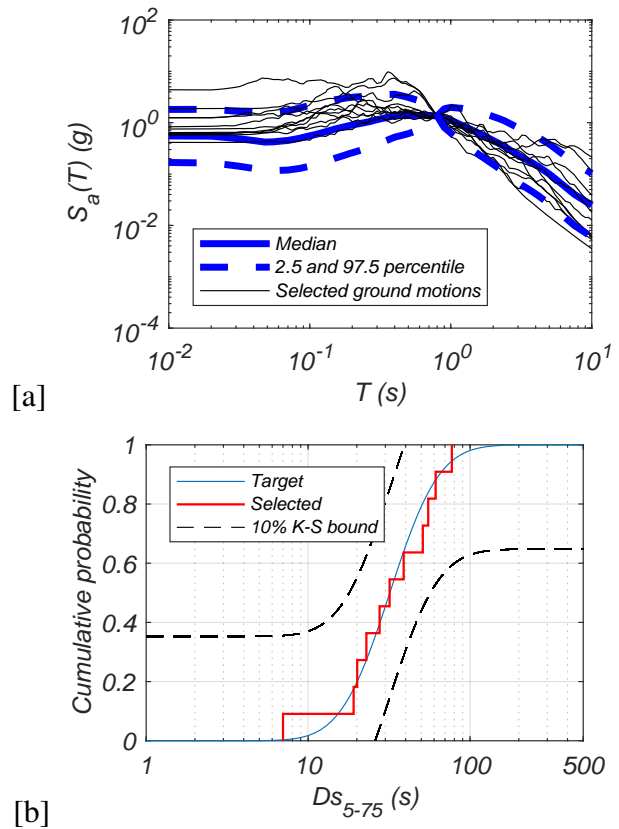
[a]

[b]

Figure 2: GM selection at 2% in 50 years exceedance $S_a(T_1 = 0.8s)$ with site-specific: (a) conditional spectra target, (b) Ds_{5-75} conditional distribution functions target.

4. CONCLUSION

A probabilistic multi-hazard earthquake-tsunami fragility assessment framework is presented in this study, which considers the effect of accumulated damage on the structure due to earthquake loading on its subsequent tsunami response. The framework involves simulating structural response using advanced 3D nonlinear FEM of the structure subjected to sequential earthquake-tsunami loading at several seismic and tsunami intensity levels, using back to back NRHA and NSP analyses. A modern earthquake-tsunami code designed four story RC SMRF building is used as an application example to illustrate the framework. Results indicate that:

• The effect of accumulated damage due to earthquake loading is more pronounced in reducing the stiffness of the structure compared to reduction in structural capacity. This accumulated damage effect on reduction in stiff-
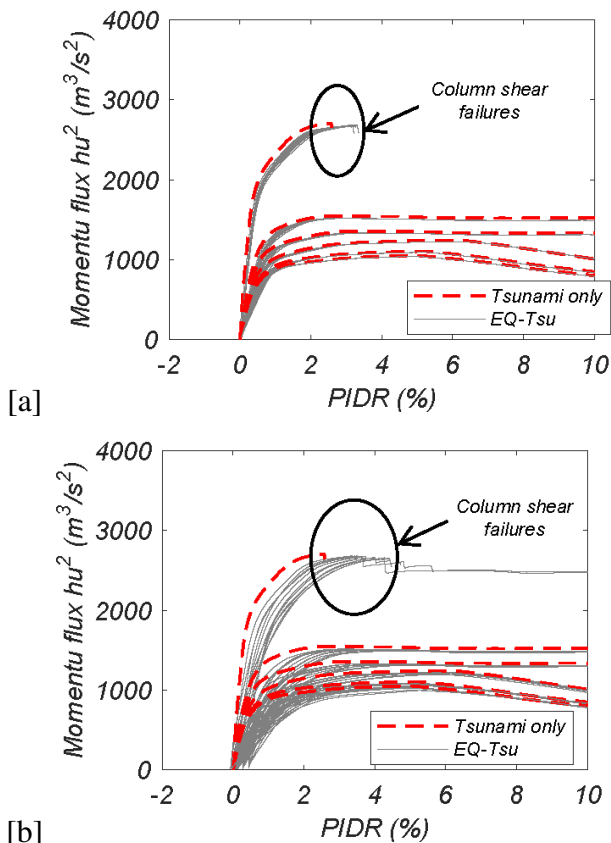
[a]

[b]

Figure 3: Effect of seismic intensity level on the lateral response of the example building (a) at 10% in 50 years $S_a(T_1)$ exceedance probability; (b) at 2% in 50 years $S_a(T_1)$ exceedance probability.
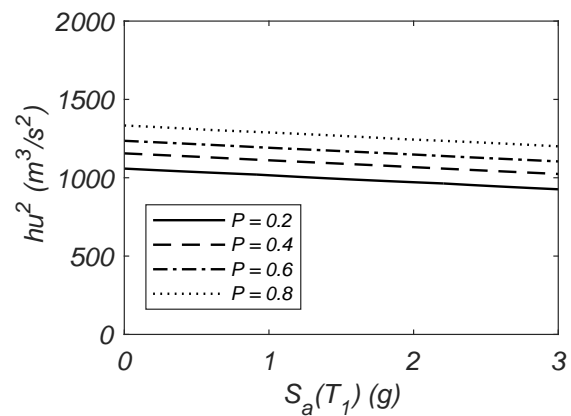

Figure 4: Parameterized joint earthquake-tsunami fragility function of the application example building as function of spectral acceleration $S_a(T_1)$ and momentum flux hu^2 for 2 % PIDR exceedance level

or views of NIST or the US Department of Commerce.

ness and strength increases with seismic intensity.

- The tsunami structural capacity required to achieve a given probability of damage exceedance decreases with increasing seismic intensity, especially at lower damage states.

The proposed framework can be extended in future for risk assessment of structures in coastal regions prone to multi-hazard earthquake-tsunami events.

5. ACKNOWLEDGEMENT

6. REFERENCES

ACI (2014). *Building code requirements for structural concrete (ACI 318-14) and commentary (ACI 318R-14)*. American Concrete Institute, Farmington Hills, Michigan.

Alam, M. S., Barbosa, A. R., Scott, M. H., Cox, D. T., and van de Lindt, J. W. (2018). "Development of physics-based tsunami fragility functions considering structural member failures." *Journal of Structural Engineering*, 144(3), 04017221.

ASCE (2016). *Minimum design loads for buildings and other structures, ASCE/SEI 7-16*. American Society of Civil Engineers, Reston,VA.

Attary, N., van de Lindt, J. W., Unnikrishnan, V. U., Barbosa, A. R., and Cox, D. T. (2017). "Methodology for development of physics-based tsunami fragilities." *Journal of Structural Engineering*, 143(5), DOI: 10.1061/(ASCE) ST.1943–541X.0001715.

Baker, J. W. and Lee, C. (2018). "An improved algorithm for selecting ground motions to match a conditional spectrum." *Journal of Earthquake Engineering*, 22(4), 708–723.

Barbosa, A. R., Ribeiro, F. L., and Neves, L. A. (2017). "Influence of earthquake ground-motion duration on

damage estimation: application to steel moment resisting frames." *Earthquake Engineering & Structural Dynamics*, 46(1), 27–49.

Belejo, A., Barbosa, A. R., and Bento, R. (2017). "Influence of ground motion duration on damage index-based fragility assessment of a plan-asymmetric non-ductile reinforced concrete building." *Engineering Structures*, 151, 682–703.

Carey, T., Mason, H., Barbosa, A., and Scott, M. (2018). "Multi-hazard earthquake and tsunami effects on soil-foundation-bridge systems." *Journal of Bridge Engineering*, (In press), DOI: 10.1061/(ASCE)BE.1943–5592.0001353.

Chandramohan, R., Baker, J. W., and Deierlein, G. G. (2016). "Impact of hazard-consistent ground motion duration in structural collapse risk assessment." *Earthquake Engineering & Structural Dynamics*, 45(8), 1357–1379.

Charvet, I., Suppasri, A., and Imamura, F. (2014). "Empirical fragility analysis of building damage caused by the 2011 Great East Japan tsunami in Ishinomaki city using ordinal regression, and influence of key geographical features." *Stochastic Environmental Research and Risk Assessment*, 28(7), 1853–1867.

Haselton, C. B., Liel, A. B., Taylor-Lange, S. C., and Deierlein, G. G. (2016). "Calibration of model to simulate response of reinforced concrete beam-columns to collapse.." *ACI Structural Journal*, 113(6).

Karthik, M. M. and Mander, J. B. (2010). "Stress-block parameters for unconfined and confined concrete based on a unified stress-strain model." *Journal of Structural Engineering*, 137(2), 270–273.

Latcharote, P. (2015). "Development of nonlinear analysis method to simulate nonlinear behavior of rc walls in rc wall-frame buildings suffering damage from earthquake and subsequent tsunami." Ph.D. thesis, Kochi University of Technology, Japan, Kochi University of Technology, Japan.

Long, Y. (2013). "Effect of subduction zone earthquakes on sdof bridge models." M.S. thesis, Oregon State University, OR, USA, Oregon State University, OR, USA.

Park, H., Cox, D. T., Alam, M. S., and Barbosa, A. (2017). "Probabilistic seismic and tsunami hazard analysis (PSTHA) conditioned on a mega-thrust rupture of the Cascadia Subduction Zone." *Frontiers in Built Environment*, 3, doi: 10.3389/fbuil.2017.00032.

Park, S., van de Lindt, J. W., Cox, D., Gupta, R., and Aguiniga, F. (2012). "Successive earthquake-tsunami analysis to develop collapse fragilities." *Journal of Earthquake Engineering*, 16(6), 851–863.

Paulay, T. and Priestley, M. J. N. (1992). *Seismic Design of Reinforced Concrete and Masonry Buildings*. Wiley, New York, NY.

PEER/ATC (2010). "Modeling and acceptance criteria for seismic design and analysis of tall buildings." *Report No. PEER/ATC 72-1*, Applied Technology Council, Redwood City, CA.

Peiris, N. (2006). "Vulnerability functions for tsunami loss estimation." *First European conference on Earthquake Engineering and Seismology, a joint event of the 13th ECEE & 30th General Assembly of the ESC), Geneva, Switzerland*, 3–8.

Petrone, C., Rossetto, T., and Goda, K. (2017). "Fragility assessment of a RC structure under tsunami actions via nonlinear static and dynamic analyses." *Engineering Structures*, 136, 36–53.

Scott, B. D., Park, R., and Priestley, M. J. N. (1982). "Stress-strain behavior of concrete confined by overlapping hoops at low and high strain rates." *Journal of American Concrete Institute*, 79(1), 13–27.

Scott, M. H. and Fenves, G. L. (2006). "Plastic hinge integration methods for force-based beam–column elements." *Journal of Structural Engineering*, 132(2), 244–252.

Scott, M. H. and Ryan, K. L. (2013). "Moment-rotation behavior of force-based plastic hinge elements." *Earthquake Spectra*, 29(2), 597–607.

Suppasri, A., Charvet, I., Imai, K., and Imamura, F. (2015). "Fragility curves based on data from the 2011 Tohoku-Oki Tsunami in Ishinomaki City, with discussion of parameters influencing building damage." *Earthquake Spectra*, 31(2), 841–868.